COMPDYN 2013
4th ECCOMAS Thematic Conference on
Computational Methods in Structural Dynamics and Earthquake Engineering
M. Papadrakakis, V. Papadopoulos, V. Plevris (eds.)
Kos Island, Greece, 12–14 June 2013

3-D CONVOLUTIONAL PERFECTLY MATCHED LAYER MODELS FOR DYNAMIC SOIL-STRUCTURE INTERACTION ANALYSIS IN THE FINITE ELEMENT TIME-DOMAIN

Bo-Qing Xu[1], Hing-Ho Tsang[2], and S. H. Lo[3]

Department of Civil Engineering, The University of Hong Kong
Pokfulam Road, Hong Kong

[1] xuboqing@hku.hk, [2] tsanghh@hku.hk, [3] hrcclsh@hku.hk

Keywords: Perfectly Matched Layer, Finite Element Method, Seismic Isolation, Dynamic Soil-Structure Interaction, Boundary Conditions.

Abstract. *The perfectly matched layer (PML) has been employed as a very efficient absorbing boundary condition for solving elastodynamic problems in bounded domains by using the finite difference method. However, in the finite element time domain (FETD), the application of PML formulations usually involves a mixed scheme with velocity/displacement and stresses as unknowns to avoid temporal convolution operations, which could lead to an increase in computational costs especially when three-dimensional (3-D) simulations are used. This paper presents the preliminary research on 3-D convolutional PML models for dynamic soil-structure interaction (SSI) analysis in FETD with displacements as the only unknowns. The variational formulation is derived for the use of finite element method (FEM) to discretize the problem domain, which avoids tricky coordinate transformation and requires minor modification of existing displacement-based finite element software. The stability and efficiency of the proposed formulation are first demonstrated by relevant 3-D benchmark examples even with small bounded domains. Numerical results are also presented for the classical SSI problem of a building with rigid footing on layers on a half-space.*

1 INTRODUCTION

A PML is an artificial absorbing layer for wave equations, commonly used to truncate computational regions in numerical methods to simulate problems with open boundaries [1]. The key property of a PML that distinguishes it from an ordinary absorbing material is that it is designed so that wave incident upon the PML from a non-PML medium does not reflect at the interface. This property allows the PML to strongly absorb outgoing waves from the interior of a computational region without reflecting them back into the interior.

The concept of a PML was first introduced to electromagnetic waves by Berenger [2] for the finite-difference time-domain (FDTD) method [3]. After the introduction of this idea, extensive research has been conducted on various aspects of PMLs for electromagnetic waves; this is mentioned without references because a review of electromagnetic PMLs is beyond the scope of this study. Most of the applications regarding PMLs are connected to FDTD, but PML has also been used in the frequency-domain finite-element method [4, 5] and more recently in the FETD method [6, 7].

PMLs have also been found applicable to other linear wave equations, for example, the Helmholtz equation [8-10], the linearized Euler equations [11], the wave equation for poroelastic media [12] and the elastodynamic wave equation [13]. The first real applications of PMLs to elastic waves were based on the split-field, velocity-stress formulation [13, 14], later extended to cases involving anisotropic media [15]. A non-splitting velocity-stress or displacement-stress approach has been suggested in which an effective recursive update strategy [16] is applied to resolve the expensive temporal convolution operations. This is known as the convolutional PML (C-PML) including the option for complex frequency shifted (CFS) [17] coordinate stretching that improves the performance of the discrete PML for near-grazing waves [18]. In the studies aforementioned, the spatial operators are approximated by finite differences. In the FETD or spectral element time-domain (SETD), the application of both split-field [19] and non-split PML [20] formulations usually involves a mixed scheme with velocity/displacement and stresses as unknowns to avoid temporal convolution operations. However, these formulations could lead to an increase in computational costs, since, apart from displacements, stresses additionally become unknowns. Since existing software for FE modeling of solid mechanics and elasticity problems usually solves for displacements only, there is a need for a PML formulation of FETD with only displacements as unknowns for the elastic second-order wave equation.

To the author's knowledge, more than four attempts to solve the above challenge have been reported. Komatitisch and Tromp [21] manage to eliminate the stress terms at the cost of splitting the displacement field into four components. Basu almost established an FE discretized second-order wave equation for the displacement in [22] although the formulation involves tricky coordinate transformations of the displacement gradients to compute the strains and the implicit time integration has to be replaced by an explicit scheme [23] to enhance the computational efficiency. Recent work by Li and Matar [24] demonstrates a C-PML model for the second-order wave equation using auxiliary memory variables to avoid the convolution operators. However in reality, each memory variable in this scheme is governed by an additional equation of first-order in which the stresses are needed. The common outcome of these formulations is rather complex implementations that necessitate fundamental re-structuring of existing FE codes. Another recent work in [25] suggests a non-split variational formulation of the C-PML for the elastic-second order wave equation with displacement as the single unknown. It shows the possibility of FE implementation of an efficient CPML to existing displacement-based FE codes to solve open-region elastic wave propagation problems.

The second section of this paper developed the 3-D C-PML formulation for FETD method and implement in the model for dynamic SSI analysis. Relevant benchmark example with small bounded domains is demonstrated in the third section to show the stability and efficiency of the proposed formulation. An interesting application of this technique can also be found about the classical SSI problem of a building with rigid footing on layers on a half-space. The conclusions are discussed in the last section.

2 3-D C-PML MODEL AND FORMULATION

2.1 Concepts of Standard PML and C-PML

The key concept of the PML is a complex frequency coordinate stretching, which maps the spartial variables onto a complex space by a complex coordinate stretching function. In a 3-D space, this function can be defined as [26]

$$x_i' = \int_0^{x_i} s_i(\tilde{x}_i, \omega)\, \mathrm{d}\tilde{x}_i, \qquad i = 1, 2, 3 \tag{1}$$

The apostrophe $(\bullet)'$ indicates the stretched version of the function, ω is the angular frequency and s_i $(i = 1, 2, 3)$ are the complex frequency shifted stretched coordinate metrics proposed by Kuzuoglu and Mittra [17]

$$s_i(x_i, \omega) = \kappa_i(x_i) + \frac{\beta_i(x_i)}{\alpha_i(x_i) + j\omega}, \qquad i = 1, 2, 3 \tag{2}$$

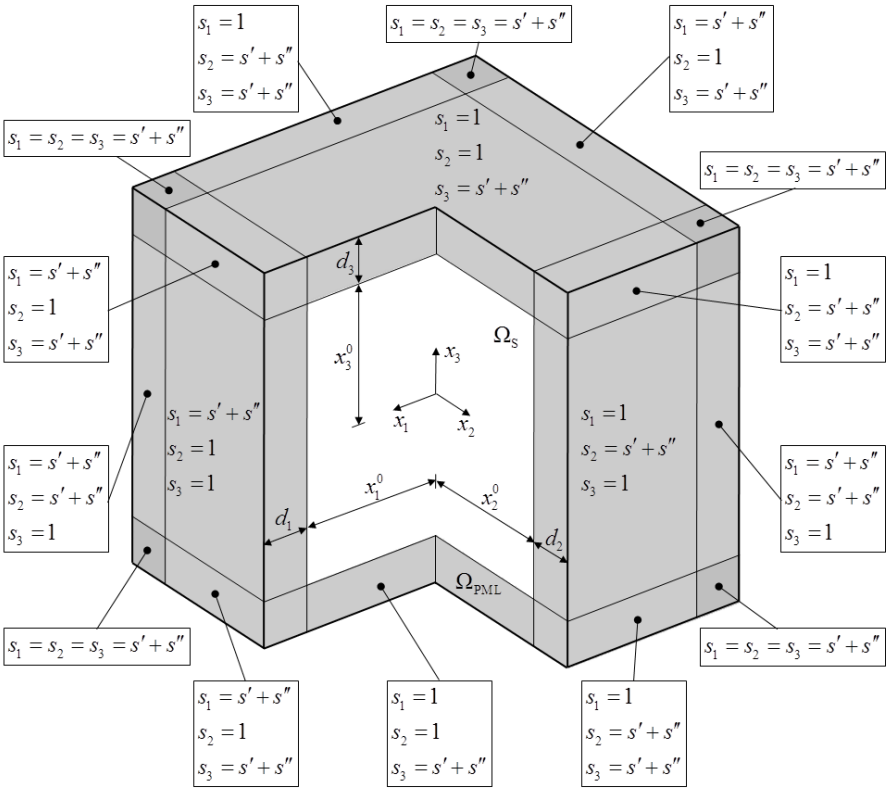

Figure 1: Computational domain truncated by Convolutional PML.

where j is the imaginary unit and κ_i, α_i and β_i are the coordinate-wise non-negative real function that controls the attenuation of the propagating waves. At the interface of the computational domain and PML, $\kappa_i = 1$ and $\beta_i = 0$. For standard PML, $\kappa_i = 1$ and $\alpha_i = 0$ in Equation (2). For the complex frequency shifted C-PML with the interface located at $x_i = x_i^0$, see Figure 1, the attenuation of the wave occurs over the PML width d_i, and continues after the remainder of the wave has been reflected from the PML boundary at $x_i = x_i^0 + d_i$. The real function $s' = \kappa_i \geq 1$ and the imaginary function $s'' = \beta / (\alpha + j\omega)$ serve to enhance attenuation of evanescent and near-grazing waves.

2.2 C-PML Equations

This paper aims at combining the 3-D C-PML model in dynamic SSI analysis. For simplicity, we consider a linear elastic medium with an open 3-D domain $\Omega = \Omega_S \cup \Omega_{PML}$, such as the one in Figure 1, in which the wave propagation is governed by

$$\text{Equation of motion: } \nabla \cdot \boldsymbol{\sigma} + \rho \mathbf{p} = \rho \ddot{\mathbf{u}} \tag{3}$$

$$\text{Strain-displacement equations: } \boldsymbol{\varepsilon} = \frac{1}{2}[\nabla \mathbf{u} + (\nabla \mathbf{u})^T] \tag{4}$$

$$\text{Constitutive equations: } \boldsymbol{\sigma} = \mathbf{C} : \boldsymbol{\varepsilon} \tag{5}$$

where $\boldsymbol{\sigma}$, $\boldsymbol{\varepsilon}$ and $\mathbf{C}$ are the stress, strain and stiffness tensors, respectively, ρ is the mass density, $\mathbf{u} = (u_1, u_2, u_3)^T$ and $\mathbf{p} = (p_1, p_2, p_3)^T$ are the displacement and body force vectors, respectively. $\nabla \cdot (\bullet)$ is the divergence operator, $\nabla (\bullet)$ represents the gradient operator and $(\bullet)^T$ represents a transpose and $(\ddot{\bullet})$ represents the second derivative with respect to time.

By introducing the complex stretched function of Equation (1) into the frequency-domain counterparts of the above governing equations and then applying the inverse Fourier transform, we can get the time-domain equation of motion and the displacement-based constitutive equations for the C-PML domain as follows

$$\nabla \cdot \boldsymbol{\sigma}' + \rho \mathbf{p} = \Psi_0(t)\mathbf{u} \tag{6}$$

$$\boldsymbol{\sigma}' = \mathbf{C}' \partial \mathbf{u} \tag{7}$$

with

$$\mathbf{C}' = \Psi_1(t)\mathbf{C}_1 + \Psi_2(t)\mathbf{C}_2 + \Psi_3(t)\mathbf{C}_3 + \Psi_4(t)\mathbf{C}_4 + \Psi_5(t)\mathbf{C}_5 + \Psi_6(t)\mathbf{C}_6 \tag{8}$$

In Equation (8), the six matrices $\mathbf{C}_i$ $(i = 1, 2, \cdots, 6)$ are given in Appendix. In Equations (6) and (8), the operators $\Psi_i(t)$ $(i = 0, 1, \cdots, 6)$ are generated by the process of the inverse Fourier transform, which are respectively given by

$$\begin{aligned} \Psi_0(t) = {} & P_0 \frac{\partial^2}{\partial t^2} + P_1 \frac{\partial}{\partial t} + P_2 + \alpha_1^2 \beta_1 P_{3,12} P_{3,13} e^{-\alpha_1 t} H(t) * \\ & + \alpha_2^2 \beta_2 P_{3,21} P_{3,23} e^{-\alpha_2 t} H(t) * + \alpha_3^2 \beta_3 P_{3,31} P_{3,32} e^{-\alpha_3 t} H(t) * \end{aligned} \tag{9}$$

$$\Psi_1(t) = \kappa_1 + \beta_1 e^{-\alpha_1 t} H(t) * \tag{10}$$

$$\Psi_2(t) = \kappa_2 + \beta_2 e^{-\alpha_2 t} H(t) * \tag{11}$$

$$\Psi_3(t) = \kappa_3 + \beta_3 e^{-\alpha_3 t} H(t) * \tag{12}$$

$$\Psi_4(t) = \frac{\kappa_1\kappa_2}{\kappa_3} + \beta_1 P_{3,12} P_{3,13}^{-1} e^{-\alpha_1 t} H(t) * + \beta_2 P_{3,21} P_{3,23}^{-1} e^{-\alpha_2 t} H(t) * - \frac{\beta_3}{\kappa_3^2} P_{4,31} P_{4,32} e^{-(\kappa_3\alpha_3+\beta_3)t/\kappa_3} H(t) * \tag{13}$$

$$\Psi_5(t) = \frac{\kappa_1\kappa_3}{\kappa_2} + \beta_1 P_{3,13} P_{3,12}^{-1} e^{-\alpha_1 t} H(t) * + \beta_3 P_{3,31} P_{3,32}^{-1} e^{-\alpha_3 t} H(t) * - \frac{\beta_2}{\kappa_2^2} P_{4,21} P_{4,23} e^{-(\kappa_2\alpha_2+\beta_2)t/\kappa_2} H(t) * \tag{14}$$

$$\Psi_6(t) = \frac{\kappa_2\kappa_3}{\kappa_1} + \beta_2 P_{3,23} P_{3,21}^{-1} e^{-\alpha_2 t} H(t) * + \beta_3 P_{3,12} P_{3,13}^{-1} e^{-\alpha_3 t} H(t) * - \frac{\beta_1}{\kappa_1^2} P_{4,12} P_{4,13} e^{-(\kappa_1\alpha_1+\beta_1)t/\kappa_1} H(t) * \tag{15}$$

where $H(t)$ is the Heaviside step function, $*$ denotes the temporal convolution and P_0, P_1, P_2, $P_{3,i}$, $P_{4,i}$ $(i = 1, 2, 3)$ are the spatially varying functions which are introduced as follows

$$P_0 = \kappa_1\kappa_2\kappa_3 \tag{16}$$

$$P_1 = \kappa_2\kappa_3\beta_1 + \kappa_1\kappa_3\beta_2 + \kappa_1\kappa_2\beta_3 \tag{17}$$

$$P_2 = \kappa_1\beta_2\beta_3 + \kappa_2\beta_1\beta_3 + \kappa_3\beta_1\beta_2 - \alpha_1\kappa_2\kappa_3\beta_1 - \alpha_2\kappa_1\kappa_3\beta_2 - \alpha_3\kappa_1\kappa_2\beta_3 \tag{18}$$

$$P_{3,ij} = \frac{\kappa_j(\alpha_i - \alpha_j) - \beta_j}{\alpha_i - \alpha_j} \quad (i, j = 1, 2, 3 \text{ and } i \neq j) \tag{19}$$

$$P_{4,ij} = \frac{\kappa_i\kappa_j(\alpha_i - \alpha_j) + \kappa_j\beta_i - \kappa_i\beta_j}{\kappa_i(\alpha_i - \alpha_j) + \beta_i} \quad (i, j = 1, 2, 3 \text{ and } i \neq j) \tag{20}$$

Note that in the computational domain Ω_S, $\kappa_i = 1$ and $\alpha_i = \beta_i = 0$ $(i = 1, 2, 3)$, herein $P_0 = 1$ and other functions in Equations (17-20) vanish. In the corner and edge regions of the C-PML, when $\alpha_i = \alpha_j$, $P_{3,ij}$ can be simplified to κ_j. By carefully choosing the spatial parameters κ_i, α_i and β_i, the singularities of $P_{4,ij}$ can be avoided. These parameters of the C-PML in the x_i direction can be chosen as suggests [20, 27, 28]

$$\kappa_i = 1 - \frac{20\Delta x_i \log_{10}(R_0)}{d_i}\left(\frac{x_i - x_i^0}{d_i}\right)^3 \tag{21}$$

$$\alpha_i = \pi\left(\frac{d_i - x_i + x_i^0}{d_i}\right) \tag{22}$$

$$\beta_i = -\frac{2v_p \log_{10}(R_0)}{d_i}\left(\frac{x_i - x_i^0}{d_i}\right)^3 \tag{23}$$

where R_0 is the theoretical reflection coefficient at normal incidence, Δx_i is the element size, v_p the longitudinal wave velocity, and x_i^0 and d_i as stated in the first part of this section are the starting location and the thickness of the C-PML, respectively.

2.3 Finite element implementation and time integration

To find a displacement-based FE solution, Equations (6-8) should be written into the weak form by using the principle of virtual work over the domain Ω with the boundary Γ

$$\int_\Omega (\delta \mathbf{u})^T \rho \Psi_0 \mathbf{u} \, d\Omega + \int_\Omega (\partial \delta \mathbf{u})^T \boldsymbol{\sigma}' \, d\Omega - \int_\Omega (\delta \mathbf{u})^T \mathbf{p} \, d\Omega - \int_\Omega (\delta \mathbf{u})^T \mathbf{T} \, d\Gamma = 0 \tag{24}$$

If we assume a free-surface boundary condition on Γ, then the contour integral in Equation (24) vanishes. By separating the convolution terms in the operators $\Psi_i(t)$, adding the external load and expanding the displacement field using FEM, we can obtain the ordinary differential equation

$$\mathbf{M}\ddot{\mathbf{d}} + \mathbf{D}\dot{\mathbf{d}} + \mathbf{K}\mathbf{d} = \mathbf{f} + \mathbf{h} + \mathbf{g} \tag{25}$$

In Equation (25), the external force vector $\mathbf{f}$ can be expressed as $\mathbf{f}(t) = -\mathbf{M}\ddot{\mathbf{d}}_{in}(t)$, when there is a time-dependent input acceleration. $\mathbf{K}$, $\mathbf{M}$, and $\mathbf{D}$ are the global stiffness, mass and damping matrices, which are assembled from the respective element matrices $\mathbf{K}^e$, $\mathbf{M}^e$, and $\mathbf{D}^e$, with the matrix entries given by

$$\begin{aligned}
\mathbf{K}_{ij}^e &= \int_{\Omega^e} \mathbf{B}_i^T \left(\kappa_1 \mathbf{C}_1 + \kappa_2 \mathbf{C}_2 + \kappa_3 \mathbf{C}_3 + \frac{\kappa_1 \kappa_2}{\kappa_3} \mathbf{C}_4 + \frac{\kappa_1 \kappa_3}{\kappa_2} \mathbf{C}_5 + \frac{\kappa_2 \kappa_3}{\kappa_1} \mathbf{C}_6 \right) \mathbf{B}_j \, d\Omega \\
&\quad + \int_{\Omega^e} \rho P_2 \mathbf{N}_i^T \mathbf{N}_j \, d\Omega \\
\mathbf{M}_{ij}^e &= \int_{\Omega^e} \rho P_0 \mathbf{N}_i^T \mathbf{N}_j \, d\Omega \\
\mathbf{D}_{ij}^e &= \int_{\Omega^e} \rho P_1 \mathbf{N}_i^T \mathbf{N}_j \, d\Omega
\end{aligned} \tag{26}$$

Here, $\mathbf{B}_j = \partial \mathbf{N}_i$ denotes the strain-displacement matrix and $\mathbf{d}$, $\dot{\mathbf{d}}$ and $\ddot{\mathbf{d}}$ are the unknown displacement, velocity and acceleration vectors, respectively. The $\mathbf{B}_j$ matrix for 3-D C-PML now reads as

$$\mathbf{B}_j = \begin{bmatrix}
N_{j,1} & 0 & 0 \\
0 & N_{j,2} & 0 \\
0 & 0 & N_{j,3} \\
N_{j,2} & N_{j,1} & 0 \\
N_{j,3} & 0 & N_{j,1} \\
0 & N_{j,3} & N_{j,2} \\
N_{j,2} & -N_{j,1} & 0 \\
N_{j,3} & 0 & -N_{j,1} \\
0 & N_{j,3} & -N_{j,2}
\end{bmatrix} \tag{27}$$

which is different from that of element inside the computational domain because the complex coordinate stretching has alternated the C-PML into an anisotropic material model. The global body force vector $\mathbf{h}$ and the global convolution vector $\mathbf{g}$ are also assembled from their respective element-level sub-vectors

$$\mathbf{h}^e = \int_{\Omega^e} \mathbf{N}^T \mathbf{p} \, \mathrm{d}\Omega \tag{28}$$

$$\begin{aligned}
\mathbf{g}^e = & -\int_{\Omega^e} \rho \mathbf{N}^T \mathbf{N} \begin{pmatrix} \alpha_1^2 \beta_1 P_{3,12} P_{3,13} e^{-\alpha_1 t} H(t) * + \alpha_2^2 \beta_2 P_{3,21} P_{3,23} e^{-\alpha_2 t} H(t) * \\ + \alpha_3^2 \beta_3 P_{3,31} P_{3,32} e^{-\alpha_3 t} H(t) * \end{pmatrix} \mathbf{d}^e \, \mathrm{d}\Omega \\
& - \sum_{k=1}^{3} \int_{\Omega^e} \mathbf{B}^T \mathbf{C}_k \mathbf{B} \; \beta_k e^{-\alpha_k t} H(t) * \mathbf{d}^e \, \mathrm{d}\Omega \\
& - \int_{\Omega^e} \mathbf{B}^T \mathbf{C}_4 \mathbf{B} \begin{pmatrix} \beta_1 P_{3,12} P_{3,13}^{-1} e^{-\alpha_1 t} H(t) * + \beta_2 P_{3,21} P_{3,23}^{-1} e^{-\alpha_2 t} H(t) * \\ - \beta_3 \kappa_3^{-2} P_{4,31} P_{4,32} e^{-(\kappa_3 \alpha_3 + \beta_3) t / \kappa_3} H(t) * \end{pmatrix} \mathbf{d}^e \, \mathrm{d}\Omega \\
& - \int_{\Omega^e} \mathbf{B}^T \mathbf{C}_5 \mathbf{B} \begin{pmatrix} \beta_1 P_{3,13} P_{3,12}^{-1} e^{-\alpha_1 t} H(t) * + \beta_3 P_{3,31} P_{3,32}^{-1} e^{-\alpha_3 t} H(t) * \\ - \beta_2 \kappa_2^{-2} P_{4,21} P_{4,23} e^{-(\kappa_2 \alpha_2 + \beta_2) t / \kappa_2} H(t) * \end{pmatrix} \mathbf{d}^e \, \mathrm{d}\Omega \\
& - \int_{\Omega^e} \mathbf{B}^T \mathbf{C}_6 \mathbf{B} \begin{pmatrix} \beta_2 P_{3,23} P_{3,21}^{-1} e^{-\alpha_2 t} H(t) * + \beta_3 P_{3,12} P_{3,13}^{-1} e^{-\alpha_3 t} H(t) * \\ - \beta_1 \kappa_1^{-2} P_{4,12} P_{4,13} e^{-(\kappa_1 \alpha_1 + \beta_1) t / \kappa_1} H(t) * \end{pmatrix} \mathbf{d}^e \, \mathrm{d}\Omega
\end{aligned} \tag{29}$$

where $\mathbf{d}^e$ is the element displacement vector.

In order to solve the differential equation for arbitrary variation of forcing function as a function of time, the most widely used methods of numerical integration in earthquake engineering are the Newmark family methods. Here we adopt one of the members of the Newmark family methods, for example, the average acceleration method, which is unconditionally stable and in the second order of accuracy. The following equation is derived for solving the displacement, velocity and acceleration at each time step Δt:

$$\begin{aligned}
\left(\frac{1}{4}\mathbf{K} + \frac{1}{\Delta t^2}\mathbf{M} + \frac{1}{2\Delta t}\mathbf{D} \right) \mathbf{d}_{t+\Delta t} = & -\left[\frac{1}{2}\mathbf{K} - \frac{2}{\Delta t^2}\mathbf{M} \right] \mathbf{d}_t - \left(\frac{1}{4}\mathbf{K} + \frac{1}{\Delta t^2}\mathbf{M} - \frac{1}{2\Delta t}\mathbf{D} \right) \mathbf{d}_{t-\Delta t} \\
& + \frac{1}{4}\mathbf{f}_{t+\Delta t} + \frac{1}{2}\mathbf{f}_t + \frac{1}{4}\mathbf{f}_{t-\Delta t} + \frac{1}{4}\mathbf{h}_{t+\Delta t} + \frac{1}{2}\mathbf{h}_t + \frac{1}{4}\mathbf{h}_{t-\Delta t} + \frac{1}{4}\mathbf{g}_{t+\Delta t} + \frac{1}{2}\mathbf{g}_t + \frac{1}{4}\mathbf{g}_{t-\Delta t}
\end{aligned} \tag{30}$$

3 NUMERICAL EXPERIMENTS

3.1 Experiment 1

To demonstrate the excellent absorbing properties of the C-PML suggested, we first attach the C-PML to five of the six faces of a cubic domain, which involves an explosive point-source residing inside the domain, see Figure 2. For the sake of simplicity, we assume the materials are homogeneous, with the density $\rho = 16500 kg/m^3$, the primary wave velocity $v_p = 100 m/s$, and the shear wave velocity $v_s = 58 m/s$. The elastic medium of 500m×500m×500m is surrounded by C-PML with the thickness of 70m. The source is located at the center of the solution domain, which is defined by

$$p(t) = 2 \times 10^7 \pi^2 (t - t_0) e^{-\pi^2 (t - t_0)} \tag{31}$$

where t_0 is the delay time. We record the horizontal and vertical displacement response in two positions R_1 and R_2 located at (-250m, 250m, 250m) and (250m, 250m, -250m), respectively. To make it convenient to compare the results to the analytical solution, we choose the direction of the source to be vertical. The FORTRAN code TI_anlytical_3D written by Dimitri Komatitsch can be used to compute the analytical solution for 3D transversely isotropic homogeneous material due to a point force source.

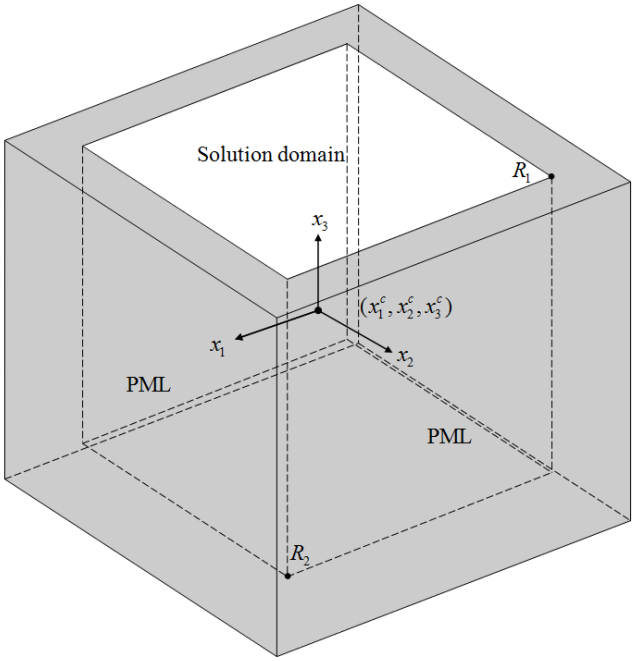

Figure 2: C-PML-truncated domain in three dimensions subjected to a point-source located at (x_1^c, x_2^c, x_3^c). R_1 and R_2 are two receivers at which the respective response is recorded.

The results of simulation with C-PML are shown in Figure 3 and Figure 4, which are compared to that of standard PML with $\alpha_i = 0$ and $\kappa_i = 1$ and the analytical solution. From all the plots, we can see the C-PML behaves perfectly in accordance with the analytical solution. Figure 5 shows some snapshots of the displacement field in the cross section of $x_1 = 0$. The displacement field magnitude here is defined as the norm $\|\mathbf{u}\| = \sqrt{u_1^2 + u_2^2 + u_3^2}$. From Figure 4, we can see that the C-PML absorbs the waves well, while the reflection of the waves from the top free surface is quite obvious after 2.0s.

3.2 Experiment 2

Typical soil-structure interaction model is used in this example as shows in Figure 6. The building structure on a 2m thick concrete foundation has a height of 24m. It is 8m in both of the other two dimensions. The superstructure is modeled by an assembly of three-dimensional frame elements. For the foundation and subsoil materials, eight-node solid elements are used in the modeling.

In order to simulate the non-reflective effects of the infinite soil transmitting half-space, the model of C-PML has been used as the boundary of the computational domain. The

numerical analysis is conducted by reducing the soil system to a 32m×32m×12m computational domain surrounded by 10m thick C-PML.

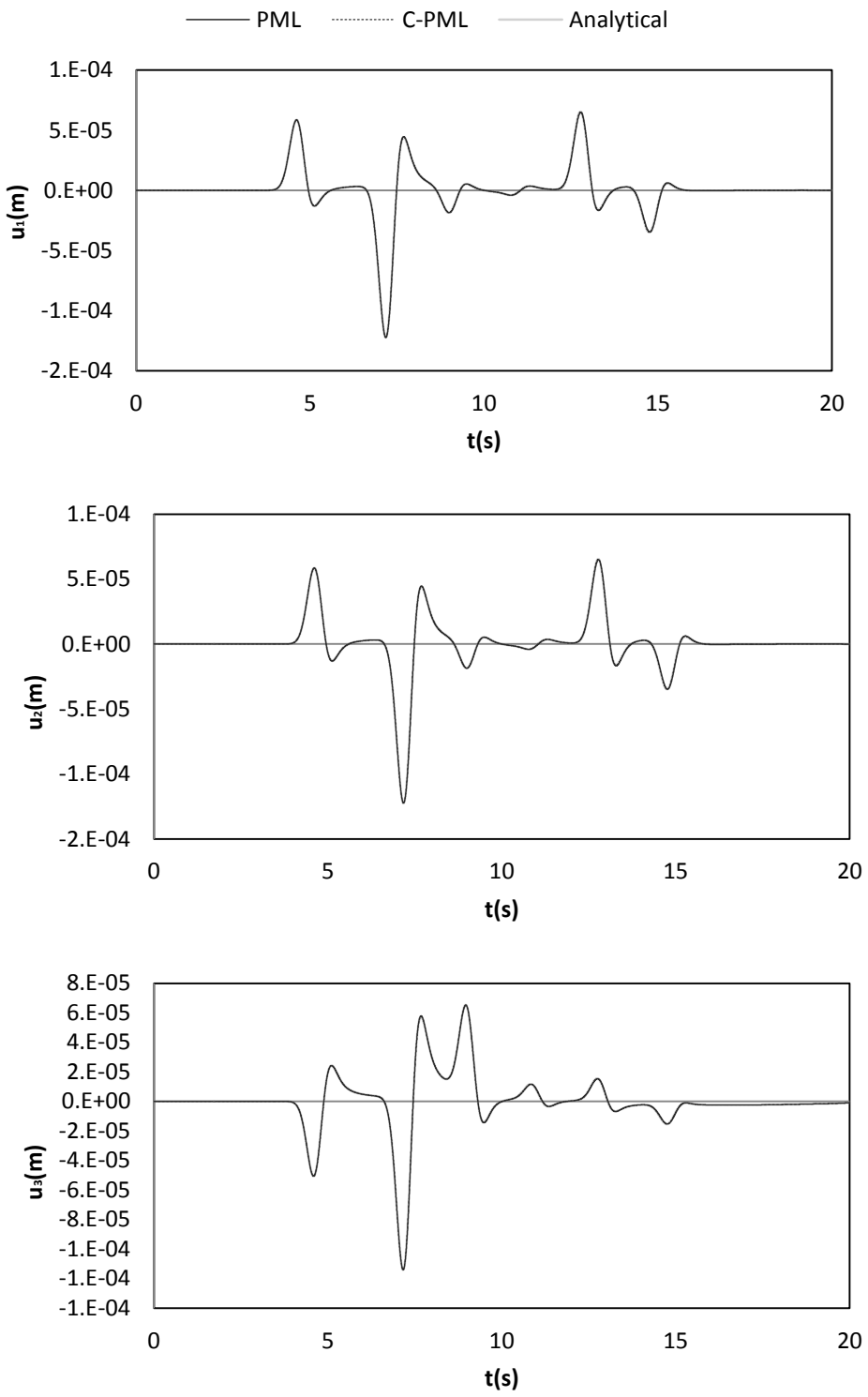

Figure 3: Comparison of the results at the receiving position R_1

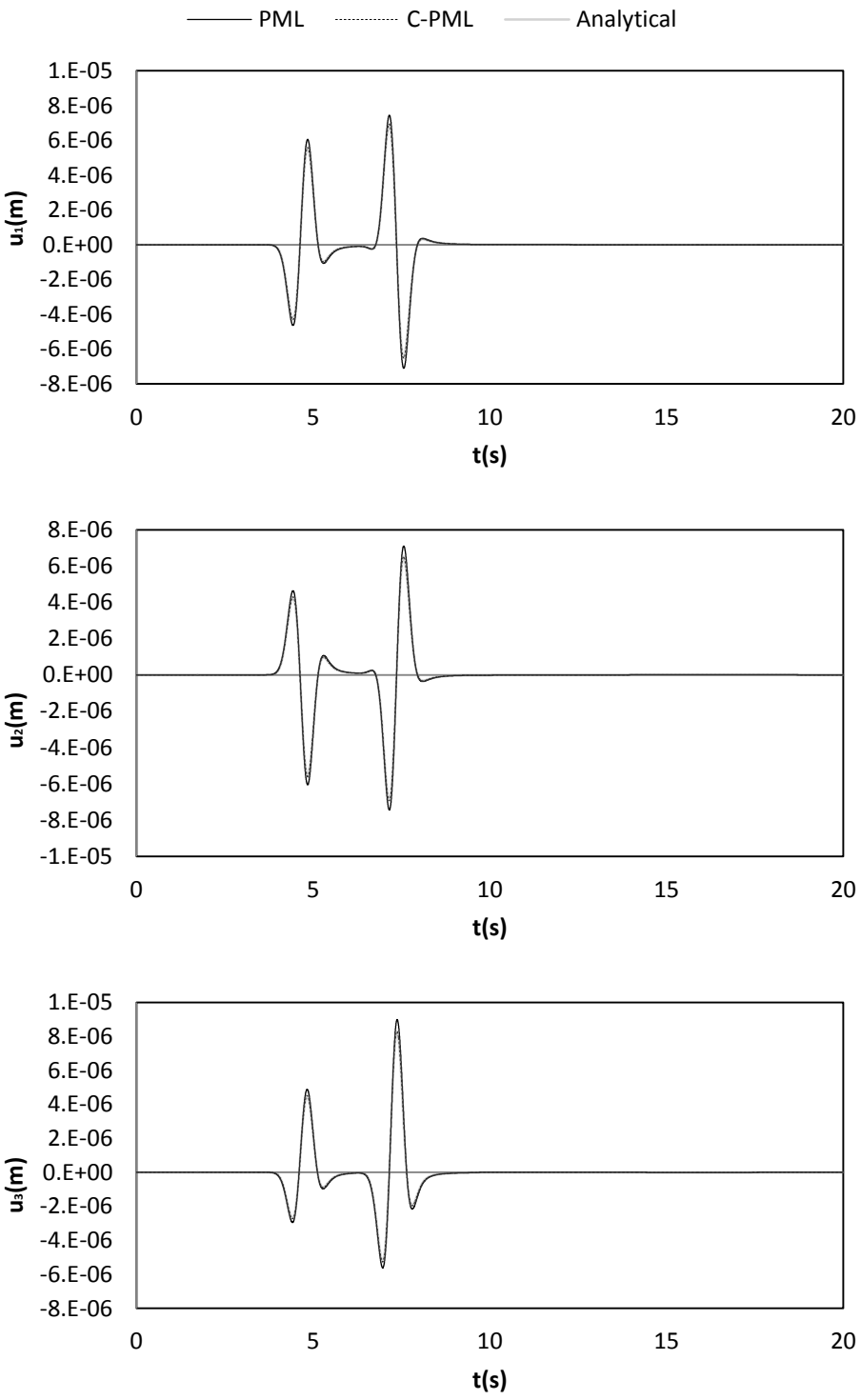

Figure 4: Comparison of the results at the receiving position R_2

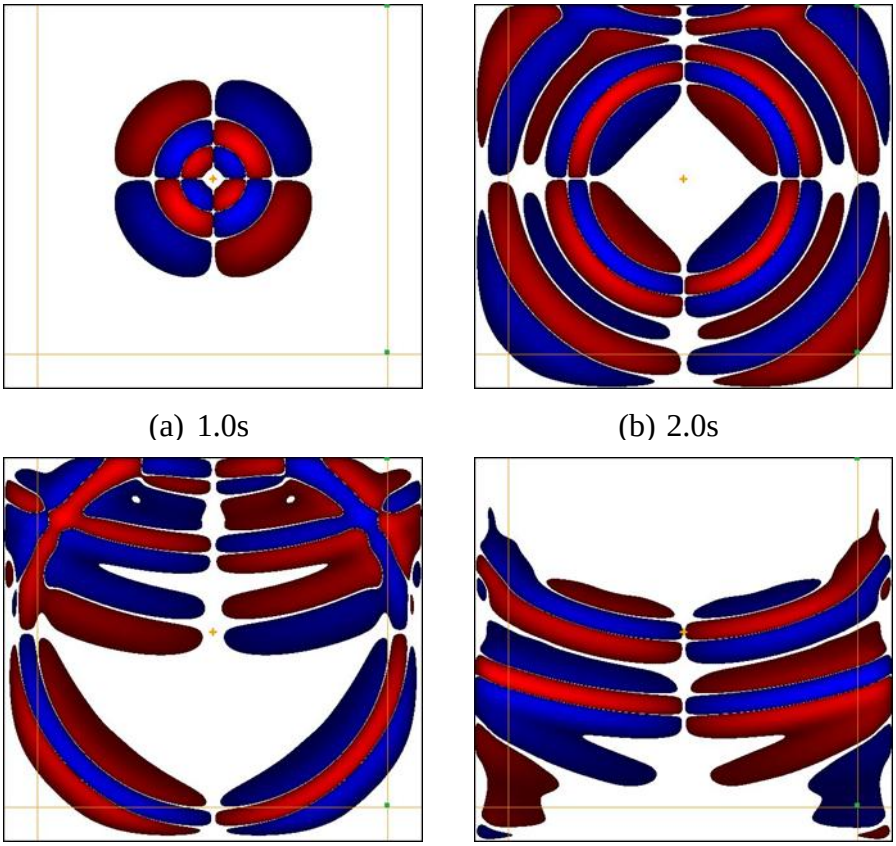

(a) 1.0s (b) 2.0s

(c) 3.0s (d) 4.0s

Figure 5: Snapshots of the displacement field magnitude of Experiment 1

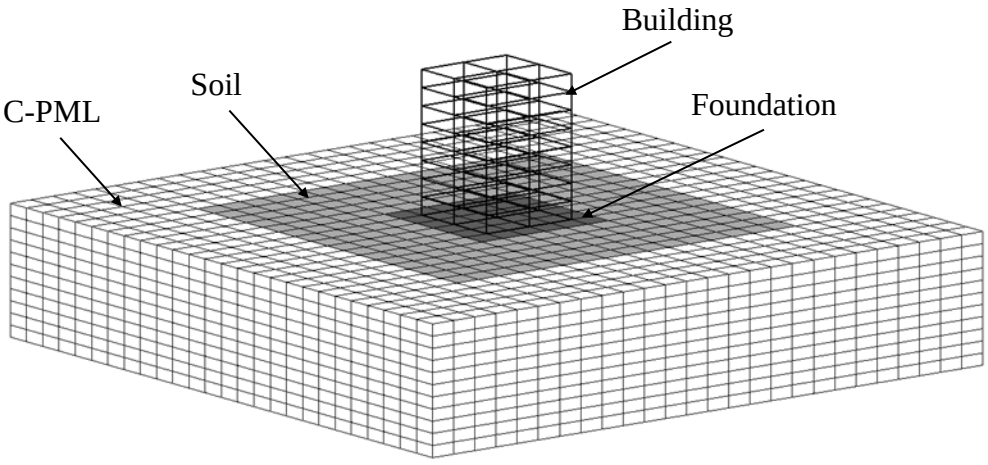

Figure 6: Finite element model of the soil-foundation-structure system with C-PML

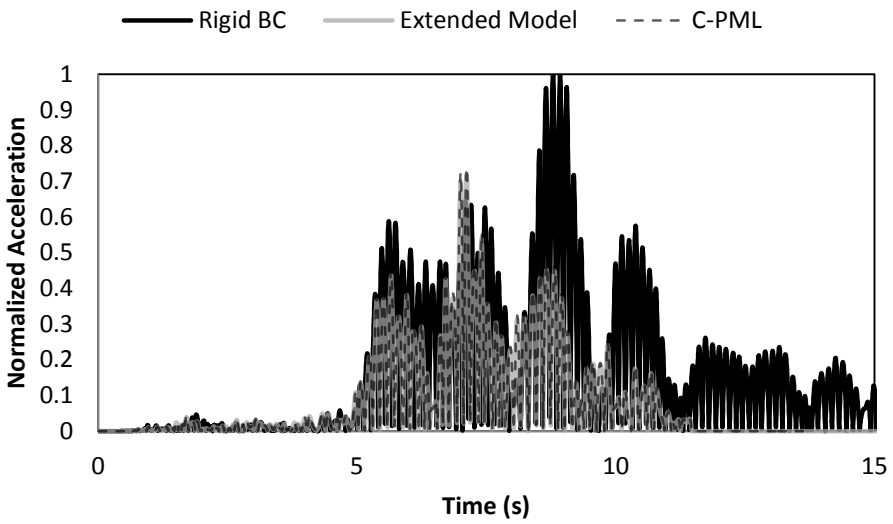

Figure 7: Footing horizontal motion

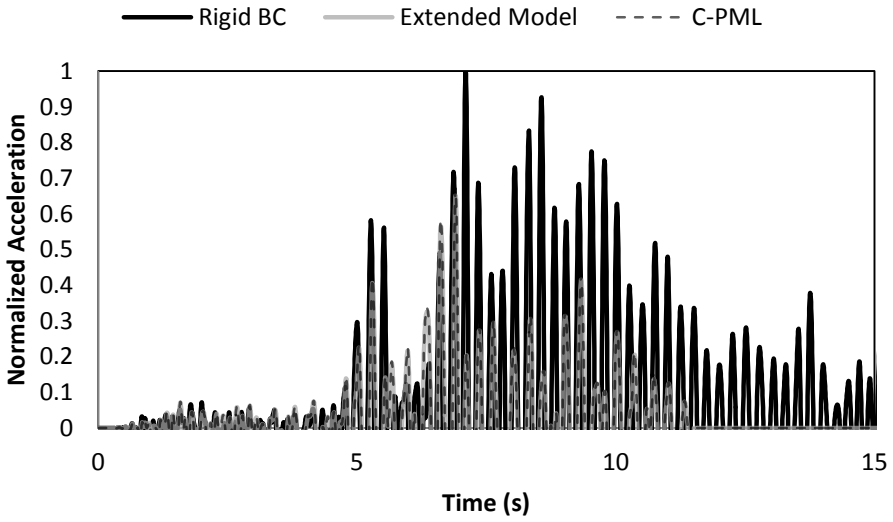

Figure 8: Roof horizontal motion

An earthquake ground motion time histories is applied at the depth of 10m. The results are compared to those from an extended model of 320m×320m×120m and those from a model with rigid boundary. Figure 7 shows the response of the center of the footing and Figure 8 shows the response of the roof. We use the norm $\ddot{u}_h = \sqrt{\ddot{u}_1^2 + \ddot{u}_2^2}$ to indicate the amplitude of horizontal motion. The results from the C-PML model are quite close to those from the extended model.

4 CONCLUSIONS

Efficient 3D C-PML models have been developed for application to dynamic soil-structure interaction analyses in time domain. It is demonstrated by numerical examples that the accuracy of the developed models is quite high. The primary purpose of this paper is to show how to implementation an efficient C-PML model to the analyses of SSI problems, when existing displacement based finite element codes need to be used to handle open-region or larger domain.

REFERENCES

[1] J.-P. Bérenger, "Perfectly Matched Layer (PML) for Computational Electromagnetics," *Synthesis Lectures on Computational Electromagnetics,* vol. 2, pp. 1-117, 2007/01/01 2007.

[2] J. P. Berenger, "A Perfectly Matched Layer for the Absorption of Electromagnetic-Waves," *Journal of Computational Physics,* vol. 114, pp. 185-200, Oct 1994.

[3] A. Taflove and S. C. Hagness, *Computational electrodynamics : the finite-difference time-domain method*, 3rd ed. Boston: Artech House, 2005.

[4] J. Y. Wu, D. M. Kingsland, J. F. Lee, and R. Lee, "A comparison of anisotropic PML to Berenger's PML and its application to the finite-element method for EM scattering," *Ieee Transactions on Antennas and Propagation,* vol. 45, pp. 40-50, Jan 1997.

[5] M. Kuzuoglu and R. Mittra, "Investigation of nonplanar perfectly matched absorbers for finite-element mesh truncation," *Ieee Transactions on Antennas and Propagation,* vol. 45, pp. 474-486, Mar 1997.

[6] D. Jiao, J. M. Jin, E. Michielssen, and D. J. Riley, "Time-domain finite-element simulation of three-dimensional scattering and radiation problems using perfectly matched layers," *Ieee Transactions on Antennas and Propagation,* vol. 51, pp. 296-305, Feb 2003.

[7] T. Rylander and J. M. Jin, "Perfectly matched layer in three dimensions for the time-domain finite element method applied to radiation problems," *Ieee Transactions on Antennas and Propagation,* vol. 53, pp. 1489-1499, Apr 2005.

[8] Q. A. Qi and T. L. Geers, "Evaluation of the perfectly matched layer for computational acoustics," *Journal of Computational Physics,* vol. 139, pp. 166-183, Jan 1 1998.

[9] E. Turkel and A. Yefet, "Absorbing PML boundary layers for wave-like equations," *Applied Numerical Mathematics,* vol. 27, pp. 533-557, Aug 1998.

[10] I. Harari, M. Slavutin, and E. Turkel, "Analytical and numerical studies of a finite element PML for the Helmholtz equation," *Journal of Computational Acoustics,* vol. 8, pp. 121-137, Mar 2000.

[11] F. Q. Hu, "On absorbing boundary conditions for linearized Euler equations by a perfectly matched layer," *Journal of Computational Physics,* vol. 129, pp. 201-219, Nov 1996.

[12] Y. Q. Zeng, J. Q. He, and Q. H. Liu, "The application of the perfectly matched layer in numerical modeling of wave propagation in poroelastic media," *Geophysics,* vol. 66, pp. 1258-1266, Jul-Aug 2001.

[13] W. C. Chew and Q. H. Liu, "Perfectly matched layers for elastodynamics: A new absorbing boundary condition," *Journal of Computational Acoustics,* vol. 4, pp. 341-359, Dec 1996.

[14] Q. H. Liu and J. P. Tao, "The perfectly matched layer for acoustic waves in absorptive media," *Journal of the Acoustical Society of America,* vol. 102, pp. 2072-2082, Oct 1997.

[15] F. Collino and C. Tsogka, "Application of the perfectly matched absorbing layer model to the linear elastodynamic problem in anisotropic heterogeneous media," *Geophysics,* vol. 66, pp. 294-307, Jan-Feb 2001.

[16] R. J. Luebbers and F. Hunsberger, "Fdtd for Nth-Order Dispersive Media," *Ieee Transactions on Antennas and Propagation,* vol. 40, pp. 1297-1301, Nov 1992.

[17] M. Kuzuoglu and R. Mittra, "Frequency dependence of the constitutive parameters of causal perfectly matched anisotropic absorbers," *Ieee Microwave and Guided Wave Letters,* vol. 6, pp. 447-449, Dec 1996.

[18] J. A. Roden and S. D. Gedney, "Convolution PML (CPML): An efficient FDTD implementation of the CFS-PML for arbitrary media," *Microwave and Optical Technology Letters,* vol. 27, pp. 334-339, Dec 5 2000.

[19] E. Becache, P. Joly, and C. Tsogka, "Fictitious domains, mixed finite elements and perfectly matched layers for 2-D elastic wave propagation," *Journal of Computational Acoustics,* vol. 9, pp. 1175-1201, Sep 2001.

[20] S. Kucukcoban and L. F. Kallivokas, "Mixed perfectly-matched-layers for direct transient analysis in 2D elastic heterogeneous media," *Computer Methods in Applied Mechanics and Engineering,* vol. 200, pp. 57-76, 2011.

[21] D. Komatitsch and J. Tromp, "A perfectly matched layer absorbing boundary condition for the second-order seismic wave equation," *Geophysical Journal International,* vol. 154, pp. 146-153, Jul 2003.

[22] U. Basu and A. K. Chopra, "Perfectly matched layers for transient elastodynamics of unbounded domains," *International Journal for Numerical Methods in Engineering,* vol. 59, pp. 1039-1074, Feb 28 2004.

[23] U. Basu, "Explicit finite element perfectly matched layer for transient three-dimensional elastic waves," *International Journal for Numerical Methods in Engineering,* vol. 77, pp. 151-176, Jan 8 2009.

[24] Y. F. Li and O. B. Matar, "Convolutional perfectly matched layer for elastic second-order wave equation," *Journal of the Acoustical Society of America,* vol. 127, pp. 1318-1327, Mar 2010.

[25] R. Matzen, "An efficient finite element time-domain formulation for the elastic second-order wave equation: A non-split complex frequency shifted convolutional PML," *International Journal for Numerical Methods in Engineering,* vol. 88, pp. 951-973, Dec 9 2011.

[26] W. C. Chew and W. H. Weedon, "A 3d Perfectly Matched Medium from Modified Maxwells Equations with Stretched Coordinates," *Microwave and Optical Technology Letters,* vol. 7, pp. 599-604, Sep 1994.

[27] G. Festa and J. P. Vilotte, "The Newmark scheme as velocity-stress time-staggering: an efficient PML implementation for spectral element simulations of elastodynamics," *Geophysical Journal International,* vol. 161, pp. 789-812, Jun 2005.

[28] F. Collino and P. B. Monk, "Optimizing the perfectly matched layer," *Computer Methods in Applied Mechanics and Engineering,* vol. 164, pp. 157-171, Oct 2 1998.

APPENDIX

$$\mathbf{C}_1 = \begin{bmatrix} 0 & 0 & 0 & 0 & 0 & 0 & 0 & 0 & 0 \\ 0 & 0 & \lambda & 0 & 0 & 0 & 0 & 0 & 0 \\ 0 & \lambda & 0 & 0 & 0 & 0 & 0 & 0 & 0 \\ 0 & 0 & 0 & 0 & 0 & 0 & 0 & 0 & 0 \\ 0 & 0 & 0 & 0 & 0 & 0 & 0 & 0 & 0 \\ 0 & 0 & 0 & 0 & 0 & \frac{\mu}{2} & 0 & 0 & 0 \\ 0 & 0 & 0 & 0 & 0 & 0 & 0 & 0 & 0 \\ 0 & 0 & 0 & 0 & 0 & 0 & 0 & 0 & 0 \\ 0 & 0 & 0 & 0 & 0 & 0 & 0 & 0 & -\frac{\mu}{2} \end{bmatrix}, \tag{32}$$

$$\mathbf{C}_2 = \begin{bmatrix} 0 & 0 & \lambda & 0 & 0 & 0 & 0 & 0 & 0 \\ 0 & 0 & 0 & 0 & 0 & 0 & 0 & 0 & 0 \\ \lambda & 0 & 0 & 0 & 0 & 0 & 0 & 0 & 0 \\ 0 & 0 & 0 & 0 & 0 & 0 & 0 & 0 & 0 \\ 0 & 0 & 0 & 0 & \frac{\mu}{2} & 0 & 0 & 0 & 0 \\ 0 & 0 & 0 & 0 & 0 & 0 & 0 & 0 & 0 \\ 0 & 0 & 0 & 0 & 0 & 0 & 0 & 0 & 0 \\ 0 & 0 & 0 & 0 & 0 & 0 & 0 & -\frac{\mu}{2} & 0 \\ 0 & 0 & 0 & 0 & 0 & 0 & 0 & 0 & 0 \end{bmatrix}, \tag{33}$$

$$\mathbf{C}_3 = \begin{bmatrix} 0 & \lambda & 0 & 0 & 0 & 0 & 0 & 0 & 0 \\ \lambda & 0 & 0 & 0 & 0 & 0 & 0 & 0 & 0 \\ 0 & 0 & 0 & 0 & 0 & 0 & 0 & 0 & 0 \\ 0 & 0 & 0 & \frac{\mu}{2} & 0 & 0 & 0 & 0 & 0 \\ 0 & 0 & 0 & 0 & 0 & 0 & 0 & 0 & 0 \\ 0 & 0 & 0 & 0 & 0 & 0 & 0 & 0 & 0 \\ 0 & 0 & 0 & 0 & 0 & 0 & -\frac{\mu}{2} & 0 & 0 \\ 0 & 0 & 0 & 0 & 0 & 0 & 0 & 0 & 0 \\ 0 & 0 & 0 & 0 & 0 & 0 & 0 & 0 & 0 \end{bmatrix}, \tag{34}$$

$$\mathbf{C}_4 = \begin{bmatrix} 0 & 0 & 0 & 0 & 0 & 0 & 0 & 0 & 0 \\ 0 & 0 & 0 & 0 & 0 & 0 & 0 & 0 & 0 \\ 0 & 0 & 2\mu+\lambda & 0 & 0 & 0 & 0 & 0 & 0 \\ 0 & 0 & 0 & 0 & 0 & 0 & 0 & 0 & 0 \\ 0 & 0 & 0 & 0 & \frac{\mu}{4} & 0 & 0 & -\frac{\mu}{4} & 0 \\ 0 & 0 & 0 & 0 & 0 & \frac{\mu}{4} & 0 & 0 & -\frac{\mu}{4} \\ 0 & 0 & 0 & 0 & 0 & 0 & 0 & 0 & 0 \\ 0 & 0 & 0 & 0 & -\frac{\mu}{4} & 0 & 0 & \frac{\mu}{4} & 0 \\ 0 & 0 & 0 & 0 & 0 & -\frac{\mu}{4} & 0 & 0 & \frac{\mu}{4} \end{bmatrix}, \tag{35}$$

$$\mathbf{C}_5 = \begin{bmatrix} 0 & 0 & 0 & 0 & 0 & 0 & 0 & 0 & 0 \\ 0 & 2\mu+\lambda & 0 & 0 & 0 & 0 & 0 & 0 & 0 \\ 0 & 0 & 0 & 0 & 0 & 0 & 0 & 0 & 0 \\ 0 & 0 & 0 & \frac{\mu}{4} & 0 & 0 & -\frac{\mu}{4} & 0 & 0 \\ 0 & 0 & 0 & 0 & 0 & 0 & 0 & 0 & 0 \\ 0 & 0 & 0 & 0 & 0 & \frac{\mu}{4} & 0 & 0 & \frac{\mu}{4} \\ 0 & 0 & 0 & -\frac{\mu}{4} & 0 & 0 & \frac{\mu}{4} & 0 & 0 \\ 0 & 0 & 0 & 0 & 0 & 0 & 0 & 0 & 0 \\ 0 & 0 & 0 & 0 & 0 & \frac{\mu}{4} & 0 & 0 & \frac{\mu}{4} \end{bmatrix}, \tag{36}$$

$$\mathbf{C}_6 = \begin{bmatrix} 2\mu+\lambda & 0 & 0 & 0 & 0 & 0 & 0 & 0 & 0 \\ 0 & 0 & 0 & 0 & 0 & 0 & 0 & 0 & 0 \\ 0 & 0 & 0 & 0 & 0 & 0 & 0 & 0 & 0 \\ 0 & 0 & 0 & \frac{\mu}{4} & 0 & 0 & \frac{\mu}{4} & 0 & 0 \\ 0 & 0 & 0 & 0 & \frac{\mu}{4} & 0 & 0 & \frac{\mu}{4} & 0 \\ 0 & 0 & 0 & 0 & 0 & 0 & 0 & 0 & 0 \\ 0 & 0 & 0 & \frac{\mu}{4} & 0 & 0 & \frac{\mu}{4} & 0 & 0 \\ 0 & 0 & 0 & 0 & \frac{\mu}{4} & 0 & 0 & \frac{\mu}{4} & 0 \\ 0 & 0 & 0 & 0 & 0 & 0 & 0 & 0 & 0 \end{bmatrix}. \tag{37}$$